



# The temporal evolution of induced seismicity sequences generated by low-pressure, long-term fluid injection

Thomas J. M. Watkins · James P. Verdon · Germán Rodríguez-Pradilla

Received: 14 June 2022 / Accepted: 21 February 2023  
© The Author(s) 2023

**Abstract** Traffic light schemes (TLSs) are commonly used to mitigate induced seismicity caused by subsurface fluid injection. Verdon and Bommer (J Seismol 25:301–326, 2021a) investigated the validity of the implicit assumptions that underpin the successful functioning of TLSs. In particular, they examined the extent to which magnitude jumps (sudden increases in event magnitudes from any preceding seismicity) and trailing events (continued increases in seismicity levels after the end of injection) took place in hydraulic fracturing (HF) induced seismicity sequences. Other technologies such as carbon capture and storage (CCS), wastewater disposal (WWD) and natural gas storage (NGS) involve the gradual but long-term injection of large fluid volumes at low pressure. Hence, we might expect to see a different spatial and temporal evolution of magnitudes for seismicity induced by low-pressure, long-term (LPLT) injections compared to HF. In this study, we compile cases of LPLT injection-induced seismicity in order to examine their temporal evolution. We examine the occurrence of magnitude jumps, trailing events and onset times for seismicity after the initiation of injection.

We find that few LPLT injections have produced trailing events, and that magnitude jumps are typically below 1.5 magnitude units. The timescale of event occurrence (relative to the onset of injection) is highly variable, likely reflecting site-specific conditions. For long-term injection, we observe a trend for the largest events to occur within the earlier part of each sequence, with magnitudes then stabilising, or even reducing, as injection continues. Finally, we evaluate the performance of the next record breaking event (NRBE) model as a method for forecasting induced event magnitudes, finding that this method performs reasonably well in most cases, but that in some cases the largest event significantly exceeds this model.

**Keywords** Induced seismicity · Traffic light schemes · Earthquake forecasting

## 1 Introduction

Earthquakes induced by subsurface fluid injection have become a significant issue for some industrial activities, including wastewater disposal (WWD), hydraulic fracturing (HF), engineered geothermal stimulation (EGS), natural gas storage (NGS) and carbon capture and storage (CCS). As the use of these technologies has increased in scale and become more widespread, more cases of injection-induced seismicity have been identified. Given the potential for damage from larger induced earthquakes and the public

---

**Supplementary Information** The online version contains supplementary material available at <https://doi.org/10.1007/s10950-023-10141-z>.

---

T. J. M. Watkins · J. P. Verdon (✉) · G. Rodríguez-Pradilla  
School of Earth Sciences, University of Bristol, Wills Memorial Building, Queen's Road, Bristol BS8 1RJ, UK  
e-mail: James.Verdon@bristol.ac.uk

concern that arises even when relatively small events are felt at the surface (e.g. Cremen and Werner 2020), there has been a growing need for decision-makers to develop strategies and regulations to limit or prevent the occurrence of induced seismicity.

The primary method used to manage induced seismicity has been traffic light schemes (TLSs). This concept was first developed by Bommer et al. (2006) to be applied to an enhanced geothermal project in El Salvador. In general, TLSs are created by defining “amber” and “red” thresholds. If the levels of seismicity are below the amber threshold then the industrial activity continues as planned. If the amber threshold is exceeded then the operator takes steps to mitigate the levels of seismicity (for example by reducing injection rates or pressures). If the red threshold is exceeded then operations are stopped.

TLSs are conceptually simple: decisions to reduce or stop injection are taken based on the magnitude of the largest event that has occurred (or the ground motions that this event has caused). TLSs are easy to explain to the general public, they are immune to model-based assumptions or parameters, and they do

not require expert judgement or interpretation once the TLS thresholds have been set.

Rational management of induced seismicity requires the identification of an appropriate risk threshold—a level of seismicity that should be minimised or prevented. This threshold can be developed by considering expected ground motions from shallow earthquakes and the exposure and vulnerability of nearby populations, buildings and infrastructure (e.g. Langenbruch et al. 2020; Schultz et al. 2020, 2021). This threshold may be very different in different situations (e.g. Kendall et al. 2019).

TLSs are retroactive: decisions are made after an event has occurred. This means that TLS thresholds must be designed by considering the potential for “magnitude jumps” and “trailing seismicity” to occur, as shown in Fig. 1. A magnitude jump describes the situation where an event occurs that is significantly larger than any previous induced seismicity during a given injection operation. Trailing seismicity describes the situation where earthquakes continue to occur and magnitudes continue to increase after injection has stopped (e.g. Kettlety et al. 2021). The occurrence of large jumps in magnitude means that

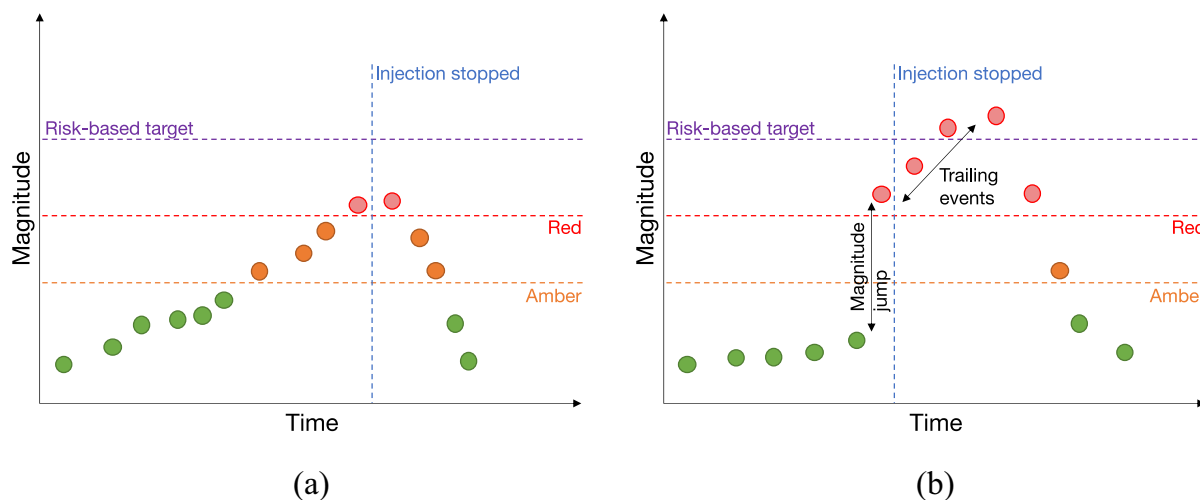


**Fig. 1** Schematic depiction of TLS operation and the potential issues caused by magnitude jumps and trailing events. In **a**, magnitudes evolve gradually through the amber and then red-light thresholds. When injection is stopped after the red-light event, magnitudes drop rapidly back to “green” levels. This behaviour is implicitly required for the safe and effective functioning of a TLS. In such situations, the red-light threshold could be set at a level that is close to the risk-based target which the TLS seeks to mitigate against. In **b**, event magni-

tudes are initially low, but a sudden jump in magnitudes produces an event that exceeds the red-light threshold. Although injection is stopped, trailing events continue to increase in magnitude for a period after injection, before eventually dropping away. In such situations, the largest event that occurs is significantly larger than the red-light threshold and a large gap between the red-light threshold and the risk-based target may therefore be required

seismicity could significantly exceed the red-light threshold before any mitigating action is taken. The occurrence of trailing seismicity means that magnitudes may continue to grow even after injection is stopped, which again means that seismicity could significantly exceed the red-light threshold at which injection was stopped.

As a result the red-light threshold should be set below the magnitude that the TLS is designed to avoid. The appropriate gap between the red-light level and the risk-based threshold will be governed by the extent to which trailing seismicity and magnitude jumps occur (Verdon and Bommer 2021a, for brevity, VB21 hereafter).

VB21 investigated these effects for HF-induced seismicity, finding that magnitude jumps were typically below 2 magnitude units and that trailing event magnitude increases occurred in approximately one quarter of cases, with the largest observed trailing event increase of 1.5 magnitude units. As such, they recommended that TLS red-light thresholds be set 2 magnitude units below the risk-based target that the TLS seeks to avoid.

In this study, we reprise the analysis presented by VB21 for cases of WWD-induced seismicity, and other cases where seismicity has been generated by low-pressure, long-term (LPLT) injection of large fluid volumes, such as NGS and CCS. To date, the WWD industry has not typically been regulated using TLSs, unlike HF and EGS. Nevertheless, many countries are planning a growth in the use of technologies such as NGS, CCS (e.g. BEIS 2018) and even hydrogen storage (e.g. BEIS 2021) in order to meet emissions targets and improve their energy security, and we anticipate that regulators may implement TLSs to manage the induced seismicity hazard posed by such developments.

WWD, CCS and NGS represent a long-term subsurface perturbation, where large volumes of fluid are injected (large WWD projects may inject millions of m<sup>3</sup>), but at a comparatively slow rate, with low injection pressures. WWD, CCS and NGS sites typically operate for years or even decades. This contrasts with HF, which represents a very short-term perturbation, where a relatively small volume of fluid is injected rapidly, at high pressure. Typically, HF is completed in a few days, and large-scale HF may inject a few tens of thousands m<sup>3</sup> per well.

We might therefore expect the temporal evolution of event magnitudes induced by LPLT fluid injection to behave in a very different manner to HF-induced seismicity. It might alternatively be argued that induced earthquake magnitudes are controlled by the properties of the pre-existing tectonic faults on which they occur (e.g. van der Elst et al. 2016), and so the temporal evolution of magnitudes could be relatively independent of the triggering process (whether short-term high-pressure HF, or LPLT injection).

## 2 Methods and analysis

We compile datasets where seismicity has been induced by WWD, NGS and CCS. Our primary objective is to assess the extent to which magnitude jumps and trailing event magnitude increases have occurred. Magnitude jumps,  $\Delta M$ , represent the gap, in magnitude units, between the largest event in the sequence at a given time, and the magnitudes of any events preceding that event.

$$\Delta M = M_i - \max(M_{[1,i-1]}) \tag{1}$$

where  $M_i$  is the magnitude of the  $i$ th event, and  $M_{[1,i-1]}$  are the magnitudes of all preceding events, and  $\Delta M$  is only computed when  $M_i > \max(M_{[1,i-1]})$ . Our focus is on the largest magnitude jump,  $\Delta M_{MAX} = \max(\Delta M)$ . Magnitude jumps can occur at any point within a sequence and  $\Delta M_{MAX}$  may not be the jump that produces the largest event.

Detection thresholds vary significantly between our case studies, and in some cases an apparent magnitude jump may in fact represent a constraint imposed by a lack of event detection. Limited detection thresholds are often apparent at the start of event sequences, whereas dedicated local monitoring arrays may be deployed, either by operators, regulators or academics, once an event sequence reaches larger magnitudes. As such, we only consider magnitude jumps that occur above a magnitude of M 2.5.

We define trailing events as increases in magnitude that occur after injection has ceased, and the maximum trailing event increase as:

$$\Delta M_T = \max(M_{T>t_E}) - \max(M_{T<t_E}) \tag{2}$$

where  $M_{T>t_E}$  are events occurring after the end of injection, and  $M_{T<t_E}$  are events occurring before the

end of injection, and only positive  $\Delta M_T$  values are considered. Schultz et al. (2022) provide observational evidence that trailing seismicity follows Båth's law for earthquake aftershocks, with  $\Delta M_T$  being proportional to the relative numbers of earthquakes during and after the injection phase.

For areas with a large number of injection wells, it can be difficult to identify specific causative wells, and therefore to establish when the influence of injection has stopped (at which point any further seismicity can be considered to be "trailing"), especially when some wells may inject for long periods before and after the sequence in question. This situation is more complex than hydraulic fracturing cases, where bursts of seismicity are more easily linked to specific wells that have brief, short-lived injection periods. Details of the wells used in our analysis with respect to injection start and stop times for each sequence are provided in the supplementary materials, but in some cases the decision to include or exclude a particular well as a contributor to a given seismic sequence is somewhat arbitrary.

The Gutenberg and Richter (1944)  $b$ -value (GR hereafter) is also a significant factor when assessing the hazard posed by induced seismicity with low  $b$ -values indicating an increased likelihood of larger magnitude events. For tectonic seismicity,  $b$ -values are commonly observed to be close to 1.0 (Frohlich and Davis 1993). However, it has been suggested that seismicity driven directly by fluid processes may produce higher  $b$ -values, implying a higher number of small events relative to the number of large events (e.g. Wyss et al. 1997; Kettlety et al. 2019). Therefore, we compute  $b$ -values for all of our datasets using the Aki (1965) maximum likelihood method and a Kolmogorov–Smirnov test to estimate the minimum magnitude of completeness,  $M_{MIN}$  (Verdon 2013).

We also analyse the time lags between the start of injection and the onset of seismicity. The observed lags prior to induced seismicity onset can inform monitoring strategies at future sites. Again, the lag between injection and seismicity may be constrained by the detection thresholds of monitoring arrays (since small, early events may be missed) and by appropriate identification of which wells were responsible for the seismicity (and so when the start of injection took place).

In their compilation of induced seismicity sequences, van der Elst et al. (2016) argued that

induced seismicity is driven primarily by regional tectonic conditions, and hence the largest event could occur at any time within a sequence. This concept poses a potential challenge for the successful use of TLSs, since TLSs implicitly depend on the assumption that magnitudes increase progressively as injection continues. The concept proposed by van der Elst et al. (2016) implies that the largest events could occur relatively early within a sequence before any mitigation actions could be taken. Van der Elst et al. (2016) tested this assertion by examining the position of the largest event within each sequence as measured by the ratio  $P_{Mmax} = N_{prior}/N$ , where  $N_{prior}$  is the number of events before the largest event, and  $N$  is the total number of events larger than the magnitude of completeness. They found no evidence to indicate that the largest event was not positioned at random within each sequence. However, subsequently both Skoumal et al. (2018) and VB21 compiled HF-induced seismicity cases and found statistically significant evidence that the largest events were positioned later within their respective sequences. The positioning of larger events later within sequences is consistent with rates and magnitudes of induced seismicity being correlated with injection volumes (e.g. Hallo et al. 2014) and, if so, larger events become more likely as the injected volume increases.

Using geomechanical simulations, Kroll and Cochran (2021) argued that the occurrence time of larger events will be determined by the stress conditions. Where stresses are further from the failure criteria, faults will reactivate slowly and larger-magnitude events will occur towards the end of the sequence, whereas when stresses are close to failure, runaway rupture will occur quickly, with large events occurring at the start of the sequence.

Here, we compile  $P_{Mmax}$  values for each LPLT injection-induced sequence. To mitigate the effects of varying detection thresholds in time for some sequences, we only evaluate the numbers of events above an  $M_{MIN}$  threshold that is appropriate for the entire timespan of the available catalogue. We use a  $\chi^2$  test to evaluate whether the observed  $P_{Mmax}$  values are consistent with the random positioning of the largest event within each sequence.

Finally, various studies have recognised the potential to use seismicity forecasting models to guide decision-making at industrial sites (e.g. Kwiatek et al. 2019; Clarke et al. 2019; Cao et al. 2020; Mancini

et al. 2021). The most common forecasting approach is to adopt some sort of scaling between injection rates and seismicity rates that can be extrapolated to forecast what may happen as injection continues. However, this approach is challenging as injection rate data is not readily available for all of our case study sites. To circumvent the necessity for injection rate data, VB21 used the next record breaking event (NRBE) approach developed by Cao et al. (2020) to evaluate whether magnitude jumps, and thereby the largest magnitude events, could be forecasted. The NRBE approach is based on record-breaking statistics theory (Tata 1969; Mendecki 2016), computed from the observed seismicity alone, and so does not require injection data. For each sequence, we compute the temporal evolution of modelled maximum magnitude,  $M_{MAX}^M$ , and compare the values of  $M_{MAX}^M$  to the actual largest event,  $M_{MAX}$ , in order to assess the degree to which the NRBE approach could provide useful magnitude forecasting.

### 3 Induced seismicity case histories

The first case of injection-induced seismicity to have been identified and studied was generated by WWD at the Rocky Mountain Arsenal, Colorado, in the mid-1960s (Evans 1966; Healy et al. 1968). Further cases of WWD-induced seismicity were identified in the USA over the following three decades, including at Perry, Ohio (Nicholson et al. 1988); Ashtabula, Ohio (Seeber et al. 2004); the Raton Basin, Colorado (Meremonte et al. 2002) and Paradox Valley, Colorado (Ake et al. 2005). It is important to note that the overwhelming majority of WWD wells have not caused induced seismicity (Verdon 2014; Walsh and Zoback 2015).

In the past two decades, the volumes of wastewater being re-injected into the subsurface in the mid-continental USA have increased substantially (Keranen et al. 2014). This increase has been driven primarily by changes in hydrocarbon production methods with a move towards reservoirs with higher water fractions and the need to dispose of flow-back fluids from hydraulic fracturing (Rubenstein and Mahani 2015). The increase in WWD in the mid-continental USA has driven significant amounts of induced seismicity in Oklahoma (Weingarten et al. 2015), Kansas (Schoenball and Ellsworth 2017), East Texas (e.g.

Frohlich 2012), the Permian Basin in west Texas (e.g. Skoumal et al. 2020a, b) and Arkansas (e.g. Horton 2012). In Oklahoma, the largest events have exceeded M 5.5, and this region has been the focus of much WWD-induced seismicity research. Cases of WWD-induced seismicity have also been observed in the Appalachian Basin (e.g. Kim 2013; Brudzinski and Kozłowska 2019) and the Western Canada Sedimentary Basin (WCSB) (e.g. Schultz et al. 2014).

In some cases, especially where both HF and WWD takes place in close proximity, it can be challenging to disentangle the causes of induced events (e.g. Yoon et al. 2017; Skoumal et al. 2018), since a reliance on simple spatial and temporal coincidence may lead to erroneous associations (e.g. Verdon and Bommer 2021b), and more detailed study of specific sequences may be required (e.g. Verdon et al. 2019; Grigoratos et al. 2022).

WWD and NGS-induced seismicity has been less common on other continents. In Europe, NGS at the Castor site, off the coast of Valencia, Spain, caused three M > 4.0 events in 2013, which led to the closure of the project (Cesca et al. 2021). Moderate magnitude induced seismicity (M < 3.0) was also generated by a high-rate WWD well in the Val d'Agri oilfield in southern Italy (Improta et al. 2015). In South America, WWD-related induced seismicity occurred in the Quifa and Rubiales oilfields in the Llanos Basin, Colombia (Molina et al. 2020), where the largest events have exceeded M > 4.0. In the Sichuan Basin, China, induced seismicity has primarily been associated with hydraulic fracturing (e.g. Lei et al. 2019). However, cases of WWD-induced seismicity have also been identified, including the Kongtan M 5.4 sequence (Lei et al. 2020) and sequences in the Rongchang (Wang et al. 2020) and Huangjiachang (Lei et al. 2013) gas fields. Induced seismicity has also been linked to the Hutubi NGS facility in Xinjiang (Tang et al. 2018).

Table 1 lists the WWD and NGS case studies compiled in our analysis. These sites were selected based on several criteria. Firstly, that magnitudes of the induced events exceeded M 3.0. Secondly, that earthquake catalogues were publicly available and contained a sufficient number of events ( $N > 30$ ) to compute a valid  $b$ -value and  $M_{MIN}$ . We sourced event catalogues either from published studies or via public networks such as TexNet (Savvaidis et al. 2019), the Oklahoma Geological Survey (Walter

**Table 1** List of case studies used in our analysis, including the year that seismicity began, the largest event size, the catalogue size ( $N$ ),  $b$ -values, magnitude jumps, trailing events,  $P_{Mmax}$ , the time of onset relative to the start of injection and the time of the largest event relative to the start of injection

Site   location	Year of onset	$M_{MAX}$	$N$	$b$	$\Delta M_{MAX}$	$\Delta M_T$	$P_{Mmax}$ [%]	$\Delta T$ (first event) [days]	$\Delta T$ (largest event) [days]	Reference
Castor   Spain	2013	4.0	3437	1.0	0.6	1.3	78	4	31	Cesca et al. (2021)
Puerto Gaitán   Colombia	2012	5.0	1637	0.9	0.5	0	87	1203	4312	Molina et al. (2020)
Rongchang   Sichuan	1980	5.6	3602	1.0	0.7	0	51	31	7014	Wang et al. (2020)
Hutubi   Xinjiang	2013	3.6	273	1.1	0.5	0	8	50	63	Tang et al. (2018)
Cordell   WCSB	1992	4.0	124	0.9	0.6	0	10	292	2008	Schultz et al. (2014)
Eagle West   WCSB	1984	4.3	91	0.8	0.5	0	36	1439	4920	Horner et al. (1994)
Graham   WCSB	2003	4.0	246	1.1	0.5	0	57	672	3194	Hosseini and Eaton (2018)
Musreau   WCSB	2018	3.9	85	0.8	0.5	0	41	251	633	Li et al. (2022)
Youngstown   Ohio	2011	4.1	282	0.9	1.3	1.3	94	15	369	Kim (2013)
Greeley   Colorado	2013	3.3	1281	0.8	0.7	0	65	220	1316	Yeck et al. (2016)
Paradox Valley   Colorado	1989	4.4	6120	0.9	0.7	0	91	15	10,108	Block et al. (2014)
Raton Basin   Colorado	1980	5.3	642	0.8	0.5	0	39	245	6139	Nakai et al. (2017)
Guy-Greenbrier   Arkansas	2009	4.7	1312	1.2	1.1	0	61	197	698	Horton (2012)
Cushing   Oklahoma	2012	5.0	501	1.1	1.3	0	74	781	2106	McGarr and Barbour (2017)
Fairview   Oklahoma	2014	5.1	2711	1.0	0.7	0	24	3096	3696	Goebel et al. (2017)
Guthrie-Langston   Oklahoma	2011	4.2	1993	1.1	0.7	0	34	2107	3152	Schoenball et al. (2018)
Pawnee   Oklahoma	2013	5.8	1525	1.1	2.1	0	33	1641	2802	Walter et al. (2017)
Prague   Oklahoma	2010	5.7	1014	0.8	0.9	0	13	6008	6883	Keranen et al. (2013)
Milan   Kansas	2014	4.9	277	0.9	1.5	0	17	199	469	Verdecchia et al. (2021)
Harper   Kansas	2014	4.3	466	0.8	0.5	0	18	846	946	Verdecchia et al. (2021)
Azle-Reno   Texas	2013	3.6	634	0.7	0.5	0	31	1624	1651	Hennings et al. (2021)
Dallas-Forth Worth   Texas	2008	3.2	64	0.6	0.3	0.2	90	60	2319	Hennings et al. (2021)
Irving   Texas	2014	3.9	818	0.8	0.5	0	30	2360	2624	Hennings et al. (2021)
Venus   Texas	2010	4.0	917	0.7	0.4	0	49	1178	3141	Hennings et al. (2021)
Timpson   Texas	2008	4.8	49	0.6	1.4	0	23	617	2116	Frohlich et al. (2014)
Cogdell   Texas	2009	4.3	285	1.1	0.5	0	38	2049	3906	Gan and Frohlich (2013)
Reeves   Texas	2018	4.9	208	0.6	1.3	0	32	809	1547	Skoumal et al. (2020b)



et al. 2020) and the USGS Comprehensive Earthquake Catalogue (ComCat). Thirdly, we sought sequences of seismicity where the onset (of both injection and seismicity) can be clearly identified. This can be challenging for WWD-induced seismicity, since high volume wells can have an influence across a wide area (Goebel et al. 2017). When considering the interacting effects between different wells in areas such as Oklahoma or west Texas, it can be difficult to isolate a particular “sequence” with a clear onset (from which subsequent magnitude jumps and delay times can be assessed), unless the entirety of WWD-induced seismicity in a particular basin were to be considered as a single sequence. Finally, in order to examine seismicity behaviour relative to the start and end of injection, we require information about, at the very least, when nearby injection wells were active. Again, given the potential areas of influence for WWD, this may require information about a significant number of wells in proximity to a given sequence. A more complete description of each case study, including the source of each event catalogue and injection start/end times, is given in the Supplementary Material. Digital event catalogues are also provided in the Supplementary Material.

## 4 Results

Table 1 lists the observations for each identified induced seismicity sequence. Figures 2, 3, 4, 5 and 6 summarise our observations across these parameters.

### 4.1 Magnitude jumps

Figure 2 shows the distribution of  $\Delta M_{MAX}$  for our case studies. We find that 75% of our cases have magnitude jumps of less than 1 magnitude unit, while only one sequence, in Pawnee, Oklahoma (Walter et al. 2017) had  $\Delta M_{MAX} > 2.0$  ( $\Delta M_{MAX} = 2.1$ ). Broadly speaking, the distribution of  $\Delta M_{MAX}$  for LPLT injection is similar to that observed for HF-induced seismicity, where  $\Delta M_{MAX} < 1$  in 60% of cases, and  $\Delta M_{MAX} > 2$  in less than 10% of cases (VB21). However, the distribution of  $\Delta M_{MAX}$  for HF-induced seismicity is shifted to slightly higher values in comparison to LPLT injection.

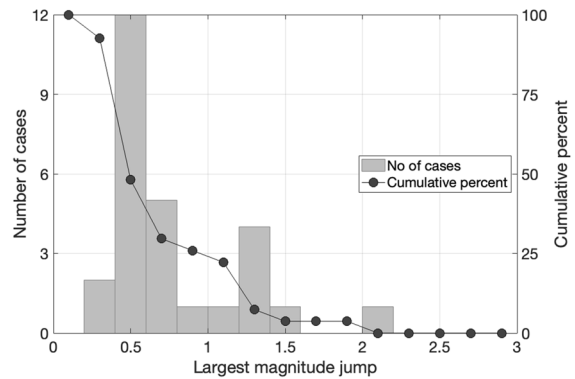


**Fig. 2** Histogram (bars) and cumulative distribution (circles) of the observed largest magnitude jumps for each of the case studies listed in Table 2

### 4.2 Trailing events

Only three sequences (11% of cases)—Castor, Youngstown and Dallas-Forth Worth—have produced trailing event magnitude increases. This is significantly fewer than for HF-induced seismicity, where 25% of cases produced trailing event magnitude increases. It is worth mentioning, however, that for the HF-induced sequences, either injection was stopped in direct response to large magnitude events or was stopped soon after large events as the stimulation operations had been completed. In contrast, for most of the LPLT injection cases injection was not terminated in response to large-magnitude events, so there is no possibility for trailing events since we define these as increases in magnitude occurring after injection is stopped. We cannot rule out the possibility that for some case studies, had injection been stopped seismicity would have continued increasing in magnitude for a period of time, generating trailing event magnitude increases. At the Castor and Youngstown sites, injection was terminated immediately in response to moderate-magnitude earthquakes and there were significant trailing event magnitude increases. The difference in observed trailing event increases between HF and LPLT injection-induced seismicity simply reflects the definition for  $\Delta M_T$  that we have used and the different timescales for HF versus LPLT injection.

VB21 observed that for HF-induced seismicity trailing events typically continued to increase in magnitude for < 1 week, with the longest example being

3 weeks. For the two LPLT injection cases with significant trailing event magnitude increases, the largest events occurred within 1 day (Youngstown) and 2 weeks (Castor) post injection, indicating that similar timescales for event magnitudes to subside might be expected for LPLT injection-induced seismicity. However, further cases where LPLT injection was immediately stopped in response to a large-magnitude event would be required to properly test this inference. As in VB21, we did not find any cases which experienced both a significant magnitude jump during injection, followed by significant trailing event increases after injection.

#### 4.3 Timescales for event initiation

Figure 3 shows histograms and cumulative distributions of time lags from the onset of injection to the first observed event and to the largest event. There is a broad range in time lags with some sites generating seismicity within a few days of injection, while other sites had time lags of up to 15 years between injection and the first observed earthquake, and some with time lags of over 25 years between the onset of injection and the largest event.

The variability in onset time likely reflects the different pore pressure and geomechanical conditions (i.e. locations of faults, stress conditions) at specific sites. In general, pore pressures will increase continually as cumulative injection volumes increase (until a steady-state is reached), and the lateral extent of the pore pressure pulse will widen with time. Hence, a critically stressed fault located very close to an injection well could be reactivated very soon after the onset of injection, whereas it will take longer for a perturbation to reach faults that are located further from the injection well. Likewise, some faults will be further from their failure state, requiring a larger pore pressure change and hence a longer time before reactivation can take place.

These results show that, while most sites that experience seismicity begin to do so within 2–3 years of injection, longer time lags can and do occur. This situation contrasts with the timescales of seismicity induced by hydraulic fracturing, which tend to appear within a few days of injection. This is because for hydraulic fracturing, fluids are injected at pressures above the tensile failure threshold for intact rock and so are, by definition, well above the pressure needed

to generate shear slip on well-orientated pre-existing faults. Hence, for hydraulic fracturing well-orientated faults can reach their failure criteria quickly after the onset of injection.

#### 4.4 $b$ -values

Figure 4 shows a histogram of  $b$ -values and the  $b$ -values as a function of the number of events in each case study population. The observed  $b$ -values range from  $0.6 \leq b \leq 1.2$ , with a mean and median slightly lower than 1.0, which is the typical value observed for tectonic seismicity (Frohlich and Davis 1993). However, in Fig. 4b we see that many of the lower  $b$ -values we obtained were from catalogues with a relatively small number of events. The precision of  $b$ -value estimates is affected by the number of events used in the calculation (e.g. Roberts et al. 2015), with  $b$ -value estimates for low numbers of events having higher uncertainties. As the numbers of events in the catalogues used to compute  $b$ -values exceeds 1000, the observed  $b$ -values fall within the range  $0.8 \leq b \leq 1.2$ .

It is interesting that the  $b$ -values we obtain for small catalogues are systematically lower than expected, rather than having any cases with elevated  $b$ -values. One possibility is that many of the catalogues used in this study have been obtained by matched filter earthquake detection (e.g. Frohlich et al. 2014; Skoumal et al. 2014). Matched filters function by identifying earthquakes with similar waveforms to reference events, which are typically selected from the largest events in a sequence. Hence, matched filters may fail to detect small events that have different locations or source mechanisms than the reference events, leading to a systematic loss of smaller events that would produce an apparent decrease in  $b$ -values.

For larger datasets, our  $b$ -values trend towards 1.0, as is the case for tectonic earthquakes. Rodríguez-Pradilla et al. (2022) found similar observations when they examined HF-induced seismicity in the WCSB. Our interpretation is that, whereas microseismicity driven by injection-induced fracturing may often have elevated  $b$ -values, once pre-existing tectonic faults begin to be reactivated, leading to larger, felt seismic events, the  $b$ -values also return to similar values to those observed for tectonic earthquakes. Detailed microseismic observations at hydraulic fracturing sites have revealed such  $b$ -value variations in practice (Kettlety et al. 2019, 2021). Hence, it is reasonable to



assume  $b$ -values of 1.0 when assessing the potential hazard posed by induced seismicity.

#### 4.5 Random occurrence of $M_{MAX}$ events?

We assess whether the largest event within each sequence occurs at a random using the approach of van der Elst et al. (2016), computing  $P_{Mmax}$  for each case and then examining whether there are any systematic trends. Figure 5 shows a histogram of  $P_{Mmax}$  for each case study and the values of  $P_{Mmax}$  as a function of  $N$ . We find that there is no correlation between  $P_{Mmax}$  and  $N$ , indicating that our results are not biased by the relative lack of detection in some datasets. A failure to detect small events early within a sequence could otherwise impose a bias to low  $P_{Mmax}$  values.

The histogram shown in Fig. 5a shows that the majority of sequences have  $P_{Mmax} < 50\%$ , implying that the largest events occur within the first half of the sequence. This contrasts with van der Elst et al. (2016), who found that  $P_{Mmax}$  was distributed randomly, and to VB21, who found that  $M_{MAX}$  was systematically shifted to the latter half of sequences for HF-induced seismicity. The distribution of  $P_{Mmax}$  observed here has a statistical significance of  $p = 17\%$  (using  $\chi^2$ ) and so we cannot rule out the null hypothesis that  $P_{Mmax}$  is distributed randomly. However, the trend for larger events to occur relatively early in the sequence is intriguing. From the observed magnitude jumps (Fig. 2) and times to seismicity onset (Fig. 3), this does not represent large events occurring without precursory activity. Instead, what we observe in many sequences is a build up to the largest event, but then magnitudes stabilising, or even reducing, as injection continues. In some cases, this may be driven by a reduction in injection rates or pressures implemented by an operator in response to induced seismicity, or even a change in injection depth to avoid near-base-ment layers (e.g. McNamara et al. 2015).

However, another possibility is that as continued injection takes place the available budget of tectonic strain is depleted, reducing the magnitudes of the subsequent events. Large magnitude induced events occur on pre-existing faults and release accumulated tectonic strain energy. For regions with relatively moderate background deformation rates, a handful of induced  $M > 3.0$  events may represent the tectonic strain accumulated over hundreds of thousands of years (e.g. Kao et al. 2018). On geological timescales,

the perturbations created by industrial activities are essentially instantaneous—there is no opportunity for tectonic stresses to re-load a fault. As such, once the induced seismicity has used up a significant portion of the accumulated tectonic strain budget, we might expect seismicity rates to reduce as injection continues.

Rodríguez-Pradilla et al. (2022) examined this effect for the WCSB using the seismic efficiency parameter,  $S_{EFF}$ , which relates the cumulative seismic moment released to the cumulative injected volume. They found that in areas prone to HF-induced seismicity, rates of seismicity that were initially elevated began to decrease as further injection continued, which they interpreted as showing that the available tectonic strain budget had been depleted. It is possible that the trend we observe here for the  $P_{Mmax}$  to fall in the earlier portion of event sequences is driven by a similar effect. However, further detailed study of seismicity rates as a function of injection volumes is required in order to assess this hypothesis.

Finally, we note that if the  $P_{Mmax}$  values shown here for LPLT injection cases are combined with the  $P_{Mmax}$  values observed by VB21 for HF cases, then the resulting distribution has nearly equal proportions of  $P_{Mmax} < 50\%$  (24 cases) and  $P_{Mmax} > 50\%$  (27 cases). Hence, the apparent randomness of  $P_{Mmax}$  observed by van der Elst et al. (2016) could be a result of the fact that their study combined HF and LPLT injection cases into a single analysis, whereas the combined observations presented here and by VB21 indicate that these different activities produce different  $P_{Mmax}$  distributions.

#### 4.6 Forecasting magnitude jumps

We use the NRBE approach (Cao et al. 2020) to evaluate whether magnitude jumps, and thereby the largest magnitude events, can be forecasted. The maximum expected magnitude jump,  $\Delta M_{MAX}$ , is determined from the observed event population with:

$$\Delta M_{MAX}^M = 2\Delta M_{MAX}^O - \sum_{i=1}^{n_j-1} \left[ \left(1 - \frac{i}{n_j}\right)^{n_j} - \left(1 - \frac{i+1}{n_j}\right)^{n_j} \right] \Delta M_i^O \tag{3}$$

where  $\Delta M_{MAX}^M$  is the modelled magnitude jump, which can be added to the largest observed event to compute the modelled magnitude of the next record breaking event,  $M_{MAX}^M$ . The observed population of

**Table 2** Best-fit and 95% confidence intervals for the log-normal distributions fitted to the LPLT, HF and synthetic  $\Delta M_{MAX}$  distributions shown in Fig. 7

Case	$\mu$	$\sigma$	$\mu_{min}$	$\mu_{max}$	$\sigma_{min}$	$\sigma_{max}$
LPLT injection	-0.35	0.48	-0.54	-0.17	0.38	0.66
HF	-0.26	0.69	-0.50	-0.01	0.56	0.92
Synthetic	0.13	0.44	0.12	0.14	0.43	0.45

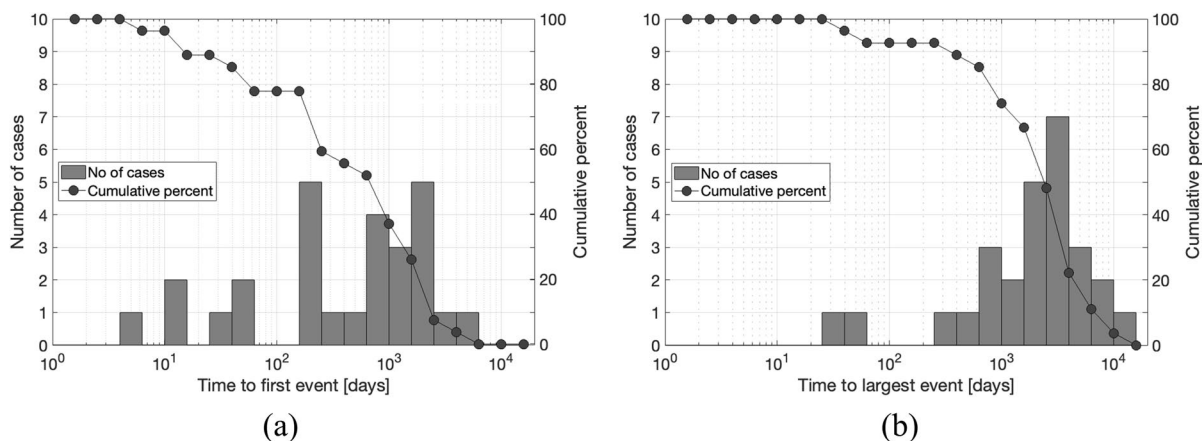


**Fig. 3** Histograms (bars) and cumulative distributions (circles) of the time between the onset of injection and **a** the first observed event and **b** the largest observed event

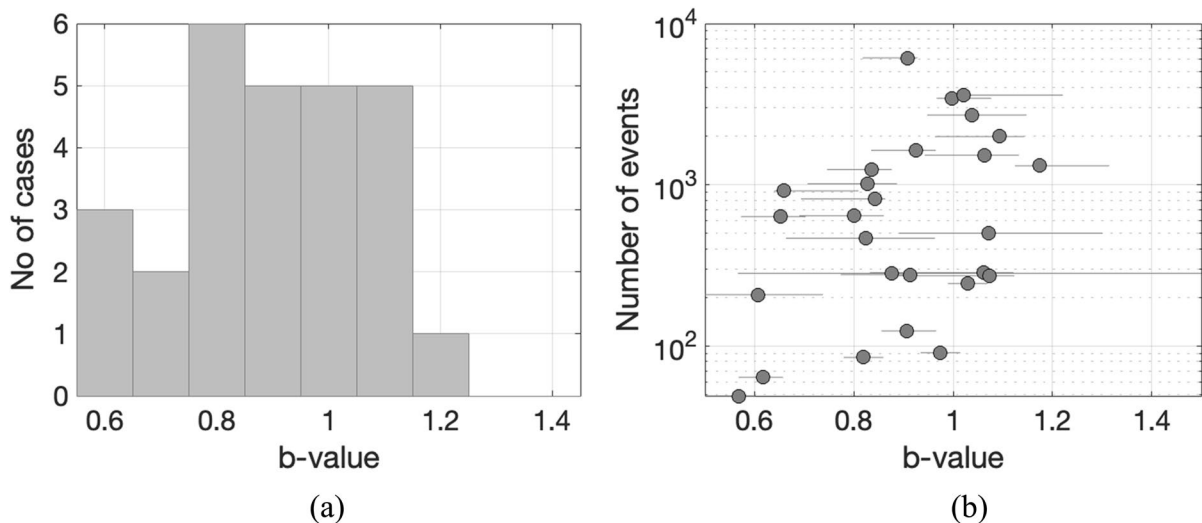


**Fig. 4** Histogram of  $b$ -values (**a**) and a cross-plot of  $b$ -values against the number of events within each event population (**b**)

magnitude jumps is given by  $\Delta M^O_i$ , where the subscript  $i$  denotes the  $i$ th value ordered by size, and  $\Delta M^O_{MAX}$  is the largest observed magnitude jump. In

this application, we compute  $\Delta M^O$  values between all earthquakes ordered from smallest to largest, irrespective of occurrence time, meaning that the

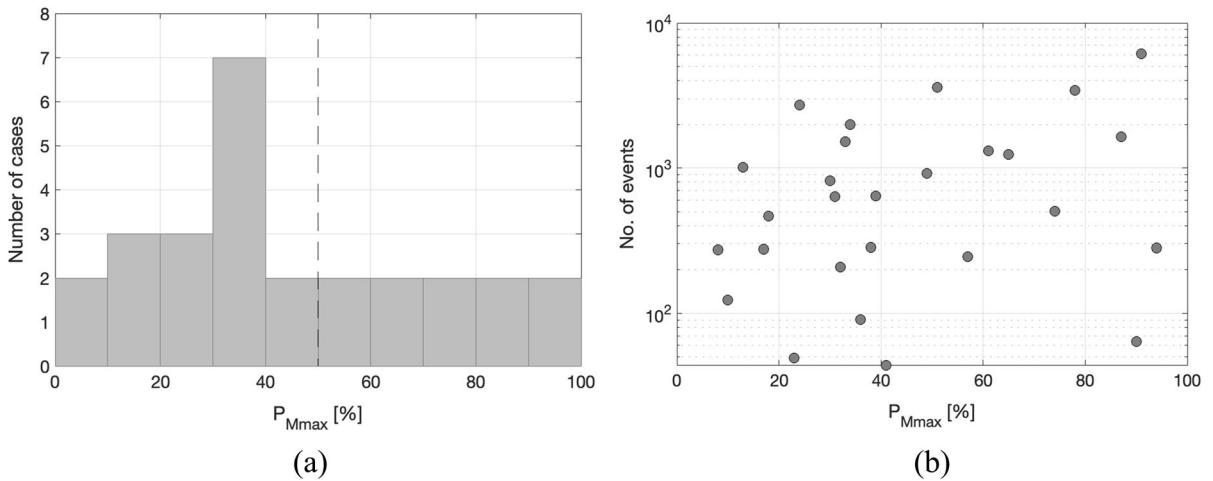


**Fig. 5** Histogram of  $P_{Mmax}$  (a) and a cross-plot of  $P_{Mmax}$  against the number of events within each event population (b)

number of magnitude jumps used in our calculation is  $n_j = N - 1$ .

Figure 6a compares the largest observed magnitude,  $M_{MAX}$ , with the NRBE forecast  $M^M_{MAX}$  prior to the occurrence of the  $M_{MAX}$  event. We note that the majority of cases fall close to or above the dashed line representing  $M^M_{MAX} = M_{MAX}$ , implying a successful forecast. However, there were 3 cases (Cordel, Milan and Timpson) where the largest event occurred before a sufficient number of events were available to generate a forecast magnitude. Likewise, two of the four

cases where  $M_{MAX}$  significantly exceeded the forecast magnitude were produced by cases with a relatively small number of total events (Youngstown,  $N = 282$ ), or a small number of events before the largest event (Prague,  $N = 136$  events before the largest event). Figure 6b shows that as the numbers of events in the catalogue increase, the forecasts generally become more accurate ( $M^M_{MAX} \geq M_{MAX}$ ). This demonstrates the importance of dedicated local monitoring networks, producing high-resolution catalogues with low detection thresholds, to guide decision-making to

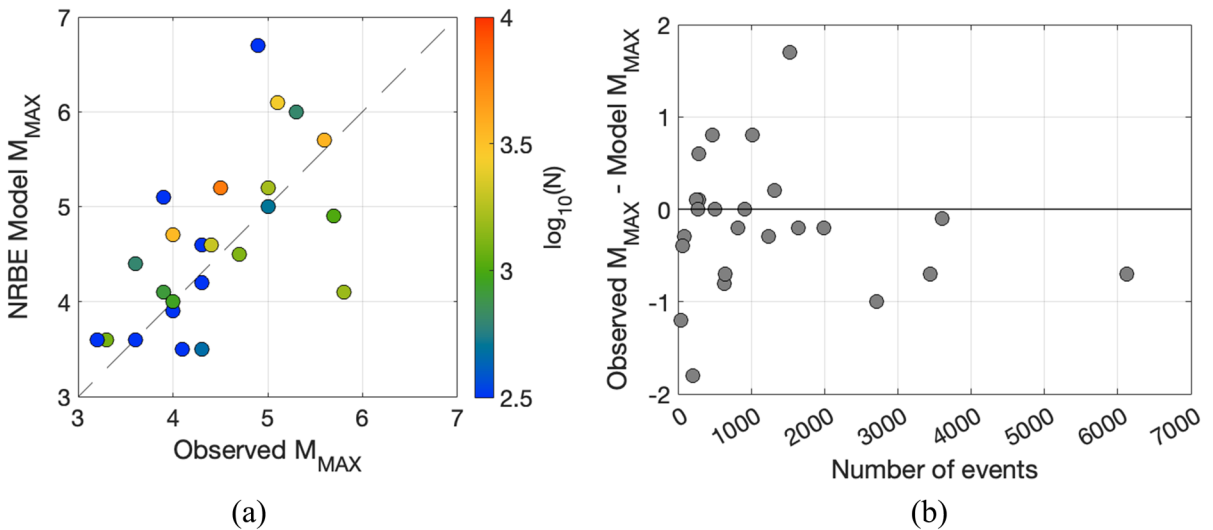


**Fig. 6** Cross-plot of observed and modelled maximum magnitudes (a), coloured by the number of events in the population, and the different between observed and modelled magnitudes as a function of the number of events (b)

mitigate induced seismicity (e.g. Kwiatek et al. 2019; Clarke et al. 2019). However, there are still cases such as the Pawnee sequence where the forecast is inaccurate despite the large number of observed events ( $N > 1500$ ). Overall, these results follow a similar pattern to that found by VB21—in general, the NRBE method produces accurate magnitude jump forecasts, indicating that the method has utility. However, occasional cases significantly exceed the modelled magnitudes implying that the approach, while useful as a guide to mitigating induced seismicity, cannot be used as an absolute guarantee that larger events will not occur.

## 5 Discussion

In Fig. 2, we examined the observed distribution of magnitude jumps ( $\Delta M_{MAX}$ ). The null hypothesis posed by van der Elst et al. (2016) is that induced seismicity is driven solely by tectonic factors, and therefore that induced event magnitudes can be treated as if they are generated at random from an underlying GR distribution. Even if magnitudes were generated at random from a GR distribution, we would still expect to see magnitude jumps leading up to the largest event, except in the extreme case where the largest event is the first to occur (which has a likelihood of  $1/N$ ). It is therefore worth examining whether our observed  $\Delta M_{MAX}$  distribution is consistent with what we might expect under the condition that event magnitudes are generated at random.

To do this, we simulate synthetic event sequences where each event magnitude is selected at random from an underlying GR distribution. We generate 1000 synthetic sequences, an example of which is shown in Fig. 7a and b. For each synthetic sequence, we set the  $b$ -value at random within a uniform range of  $0.7 < b < 1.2$ , matching the distribution of  $b$ -values from our case studies, and we set  $M_{MIN} = 1.5$ . For each sequence, we sequentially draw  $N = 1000$  events (close to the mean value of  $N$  for our observed cases) from the GR distribution and compute the resulting values of  $\Delta M$  and thereby  $\Delta M_{MAX}$ . Figure 7c and d show the resulting distribution of  $\Delta M_{MAX}$  values produced by random draws from the GR distribution, providing a comparison with the observed  $\Delta M_{MAX}$  values for this study and for the HF-induced seismicity cases in VB21. We

find that  $\Delta M_{MAX}$  values for the synthetic sequences are systematically larger than those from the HF and LPLT observations.

The synthetic and observed populations can be reasonably modelled with log-normal distributions, as shown in Fig. 7c and d. Table 2 lists the best-fit log-normal means and standard deviations for each of the LPLT, HF and synthetic  $\Delta M_{MAX}$  distributions, and their 95% confidence intervals. The differences in the log-normal means between the observed and the synthetic cases is significant: the  $\Delta M_{MAX}$  values we have observed for both HF and LPLT injection are lower than expected under the hypothesis that event magnitudes are generated at random from an underlying GR distribution. Instead, these results are consistent with the concept that event magnitudes are increasing through time as the subsurface perturbation increases in size and scale, resulting in smaller magnitude jumps as the sequence evolves.

The  $\Delta M_{MAX}$  distributions for LPLT injection- and HF-induced seismicity are similar, with HF-induced seismicity having a slightly higher mean and standard deviation, thereby producing more cases at the high  $\Delta M_{MAX}$  end of the distribution. However, there is significant overlap in the confidence intervals for the HF and LPLT cases. The similarities in  $\Delta M_{MAX}$  distributions for LPLT injection and HF-induced seismicity suggest that the tectonic conditions and frictional properties of the faults themselves have a significant control on the growth and escalation of event magnitudes. VB21 produced circumstantial evidence that large magnitude jumps might be more common on faults with high shear stresses, and Kettley et al. (2021) have shown that, for similar faults subjected to similar perturbations, the escalation of event magnitudes is strongly dependent on the orientation of the faults with respect to the in situ stress field. However, the slightly higher  $\Delta M_{MAX}$  values observed for HF-induced seismicity may indicate that high-pressure, short duration injection-induced perturbations may produce slightly larger magnitude jumps than low-pressure long-term injection.

As an additional comparison between our observed cases and the synthetic models, we examine the respective distributions of  $\Delta M$  values (Fig. 8). These distributions are compiled from all  $\Delta M$  values (i.e. not just the largest  $\Delta M_{MAX}$  value) for each case study and from each synthetic modelled sequence. Where event magnitudes are independently drawn from a GR distribution, as

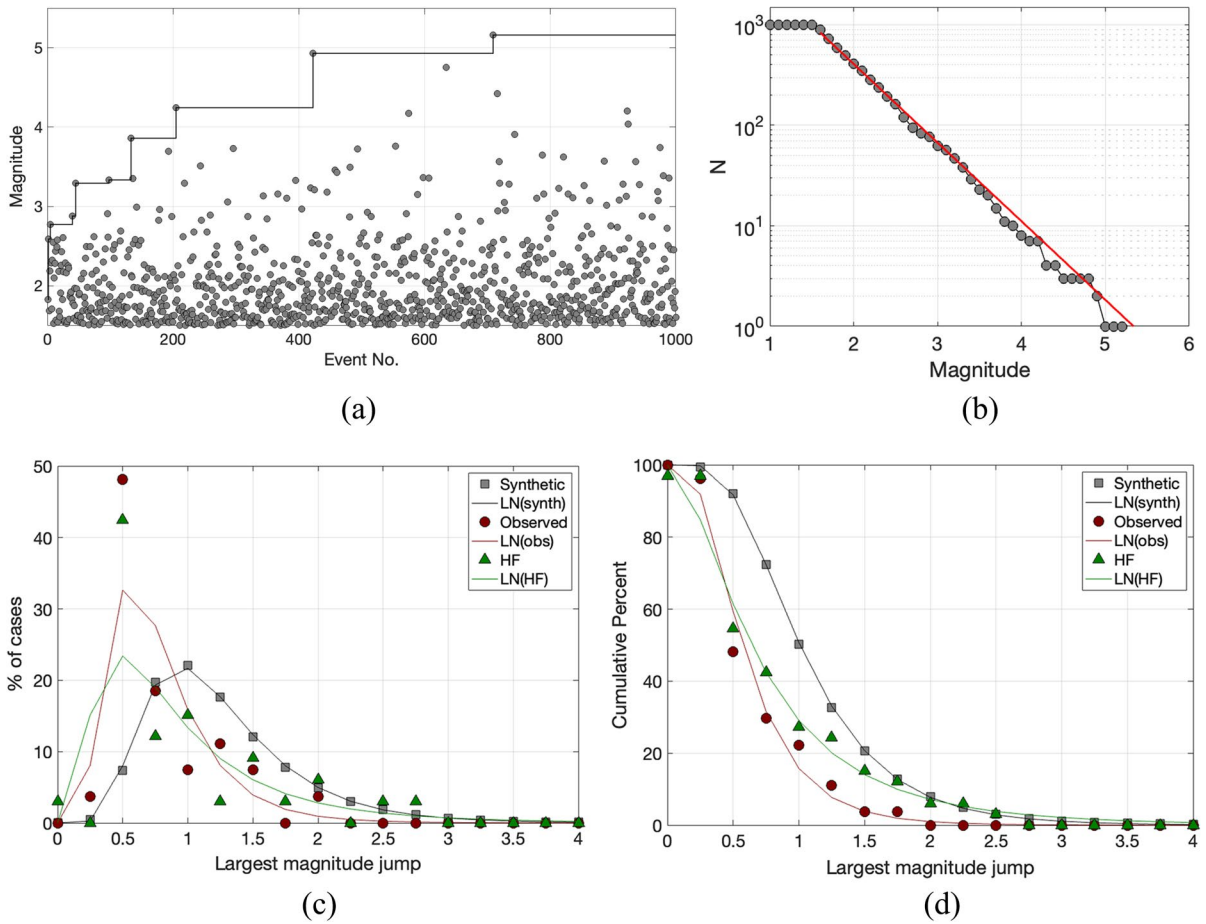


**Fig. 7** Comparison of observed and synthetic  $\Delta M_{MAX}$  distributions. In **a**, we show a representative sequence of events with magnitudes drawn at random from an underlying GR distribution given in **b**. The black line in **a** shows the magnitude jumps generated in the synthetic sequence. In **c**, we show the

distributions and **d** cumulative distributions of  $\Delta M_{MAX}$  for our observed LPLT cases (red circles), the HF cases compiled by VB21 (green triangles), and the synthetic populations (grey squares), and the best-fit log-normal distributions (red, green and black lines)

per our synthetic models, we would expect to observe a similar power-law distribution of  $\Delta M$  values, with the same exponent,  $b'$ , as the magnitude distribution (e.g. van der Elst 2021). We find that the exponent for the synthetic  $\Delta M$  distribution behaves as expected, with a power law fit across 5 orders of magnitude with  $b'=0.82$ , which is within the range of  $b$ -values used to generate the synthetic event populations. In contrast, the  $b'$  value for the compilation of observed cases is  $b'=1.32$ . This is significantly higher than any of the  $b$ -values observed for the individual case studies (Fig. 4).

The elevated  $b'$  value of the observed  $\Delta M$  distribution implies a relative absence of higher  $\Delta M$  values

relative to that expected for events drawn independently from a GR distribution. Again, this is consistent with the concept that event magnitudes increase sequentially as the subsurface perturbation increases in size and scale, resulting in smaller magnitude jumps that would be the case if events were drawn independently from an underlying GR distribution.

### 5.1 Implications for TLSs for LPLT injection sites

Our results indicate that induced seismic event magnitudes do tend to increase systematically as the subsurface perturbations generated by low-pressure, long-term injection develop. This implies that TLSs could be used



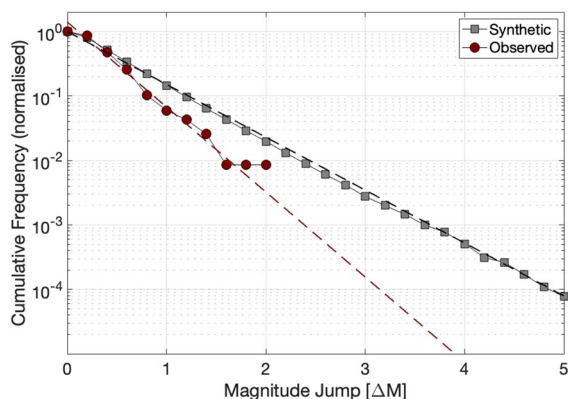


**Fig. 8** Cumulative distribution of all magnitude jumps across all of the case study sites (red circles) and those generated by our synthetic modelling (i.e. events drawn at random from a GR distribution), with power-law fits to each distribution (dashed lines)

as a tool for mitigation of seismicity from such sites. Based on our observed  $\Delta M_{MAX}$  values, we suggest that for TLSs applied to LPLT injection-induced seismicity, a reasonable red-light threshold should be set between 1.5 and 2 magnitude units below the risk-based threshold that is to be avoided. This is slightly lower than the 2–2.5 unit gap for HF-induced seismicity suggested by VB21, reflecting the slightly lower distribution of  $\Delta M_{MAX}$  observed for LPLT injection-induced seismicity. These values are similar to the proposed TLS thresholds developed by Schultz et al. (2020, 2021).

## 6 Conclusions

We anticipate that TLSs will be used to mitigate induced seismicity from future LPLT injection projects such as CCS sites and NGS facilities. Since TLSs are retroactive, an appropriate gap should be set between the red-light threshold and the magnitude of seismicity that the TLS is designed to mitigate. This gap should be based on observations of magnitude jumps and trailing events produced by operations at analogue sites. In this study, we compile datasets of LPLT injection-induced seismicity sequences, comprising primarily of WWD, with some NGS cases. We investigate the occurrence of magnitude jumps and trailing events within these datasets, finding that magnitude jumps are typically below 2.0 magnitude units. Few cases have trailing events, primarily because there are few cases where LPLT

injection has been stopped in the immediate aftermath of large-magnitude seismicity. In many of our cases, injection has continued until the present day, by definition precluding entirely the possibility of having trailing events. The distribution of  $\Delta M_{MAX}$  values is significantly different to what would be generated by random population of event magnitudes from an underlying GR distribution, indicating that event magnitudes do escalate during injection as injected volumes and event numbers increase. However, we also found that the largest events were systematically distributed within the earlier part of event sequences. This finding reflects the fact that for many of our cases, after initial escalation of magnitudes, levels of seismicity have since stabilised at lower magnitudes with continued injection. We hypothesise that this could be a result of initial release of tectonic stresses that abates as the accumulated tectonic energy is used up, but further investigation is required to assess this hypothesis in detail. We also examine the timescales over which induced seismicity begins and escalates, finding a wide range in time from the start of injection to the onset of seismicity, likely resulting from variable in situ geological conditions. Finally, we investigated the use of the NRBE approach as an alternative means to guide proactive decision-making to mitigate induced seismicity. We found that this method broadly performs well in forecasting expected event magnitudes, but for some cases the observed events significantly exceeded the model forecasts.

**Acknowledgements** The authors would like to thank NERC for funding the UKUH project, under whose auspices this work was completed. We also thank Prof. Julian Bommer for the discussions that seeded the lines of inquiry ultimately leading to this work.

**Author contribution** All the authors have contributed significantly to the development of the paper. The lead author (TJM) is a Masters student, who performed this analysis as part of his thesis. JPV and GRP supervised the lead author and contributed to the compilation of datasets used in the study. JPV wrote the paper, and GRP edited the paper.

**Funding** James Verdon and Germán Rodríguez-Pradilla's contributions to this study were funded by the Natural Environment Research Council (NERC) under the UK Unconventional Hydrocarbons Project (UKUH), Challenge 2 (Grant No. NE/R018162/1).

**Data availability** The dataset used in this study are drawn from publicly available databases or published studies. Details of each data source are provided in the Supplementary



Materials. Digital earthquake catalogues for each case study are also provided in the Supplementary Materials.

## Declarations

**Ethics approval and consent to participate** Not applicable to this study.

**Consent for publication** All the authors have reviewed the final manuscript and consent to publication in its present form.

**Competing interests** TJMW and GRP declare no competing interests. JPV has acted as an independent consultant for a variety of organisations including hydrocarbon operating companies and governmental organisations on issues pertaining to induced seismicity. None of these organisations had any input into the development, analysis or conclusions of this study.

**Open Access** This article is licensed under a Creative Commons Attribution 4.0 International License, which permits use, sharing, adaptation, distribution and reproduction in any medium or format, as long as you give appropriate credit to the original author(s) and the source, provide a link to the Creative Commons licence, and indicate if changes were made. The images or other third party material in this article are included in the article's Creative Commons licence, unless indicated otherwise in a credit line to the material. If material is not included in the article's Creative Commons licence and your intended use is not permitted by statutory regulation or exceeds the permitted use, you will need to obtain permission directly from the copyright holder. To view a copy of this licence, visit <http://creativecommons.org/licenses/by/4.0/>.

## References

- Ake J, Mahrer K, O'Connell D, Block L (2005) Deep-injection and closely monitored induced seismicity at Paradox Valley, Colorado. *Bull Seismol Soc Am* 95:664–683
- Aki K (1965) Maximum likelihood estimate of  $b$  in the formula  $\log N = a - bM$  and its confidence limits. *Bull Earthq Res Inst Univ Tokyo* 43:237–239
- BEIS (2018) The UK carbon capture, usage and storage (CCUS) deployment pathway: an action plan. Department for Business, Energy and Industrial Strategy. 75pp. Available at: <https://www.gov.uk/government/publications/the-uk-carbon-capture-usage-and-storage-ccus-deployment-pathway-an-action-plan>, last accessed 11/04/2022
- BEIS (2021) UK hydrogen strategy. Department for Business, Energy and Industrial Strategy. 120pp. Available at: <https://www.gov.uk/government/publications/uk-hydrogen-strategy>, last accessed 11/04/2022
- Block LV, Wood CK, Yeck WL, King VM (2014) The 24 January 2013  $M_L$  4.4 earthquake near Paradox, Colorado, and its relation to deep well injection. *Seismol Res Lett* 85:609–624
- Bommer JJ, Oates S, Cepeda JM, Lindholm C, Bird JF, Torres R, Marroquín G, Rivas J (2006) Control of hazard due to seismicity induced by a hot fractured rock geothermal project. *Eng Geol* 83:287–306
- Brudzinski MR, Kozłowska M (2019) Seismicity induced by hydraulic fracturing and wastewater disposal in the Appalachian Basin, USA: a review. *Acta Geophys* 67:351–364
- Cao N-T, Eisner L, Jechumtálová Z (2020) Next record breaking magnitude for injection induced seismicity. *First Break* 38:53–57
- Cesca S, Stich D, Grigoli F, Vuan A, López-Comino JÁ, Niemi P, Blanch E, Dahm T, Ellsworth WL (2021) Seismicity at the Castor gas reservoir driven by pore pressure diffusion and asperities loading. *Nat Commun* 12:4783
- Clarke H, Verdon JP, Kettlety T, Baird AF, Kendall J-M (2019) Real time imaging, forecasting and management of human-induced seismicity at Preston New Road, Lancashire, England. *Seismol Res Lett* 90:1902–1915
- Cremen G, Werner MJ (2020) A novel approach to assessing nuisance risk from seismicity induced by UK shale gas development, with implications for future policy design. *Nat Hazards Earth Syst Sci* 20:2701–2719
- Evans DM (1966) The Denver area earthquakes and the Rocky Mountain Arsenal disposal well. *Mount Geol* 3:23–36
- Frohlich C (2012) Two year survey comparing earthquake activity and injection-well locations in the Barnett Shale. *Proc Natl Acad Sci* 109:13934–13938
- Frohlich C, Davis S (1993) Teleseismic  $b$ -values - or, much ado about 1.0. *J Geophys Res* 98:631–644
- Frohlich C, Ellsworth W, Brown WA, Brunt M, Luetgert J, MacDonald T, Walter S (2014) The 17 May 2012  $M$  4.8 earthquake near Timpson, East Texas: an event possibly triggered by fluid injection. *J Geophys Res* 119:581–593
- Gan W, Frohlich C (2013) Gas injection may have triggered earthquakes in the Cogdell oil field, Texas. *Proc Natl Acad Sci* 110:18786–18791
- Goebel THW, Weingarten M, Chen X, Haffener J, Brodsky EE (2017) The 2016  $M_W$  5.1 Fairview, Oklahoma earthquakes: evidence for long-range poroelastic triggering at >40 km from fluid disposal wells. *Earth Planet Sci Lett* 472:50–61
- Grigoratos I, Savvaidis A, Rathje E (2022) Distinguishing the causal factors of induced seismicity in the Delaware basin: hydraulic fracturing or wastewater disposal. *Seismol Res Lett* in press
- Gutenberg B, Richter C (1944) Frequency of earthquakes in California. *Bull Seismol Soc Am* 34:591–610
- Hallo M, Oprsal I, Eisner L, Ali MY (2014) Prediction of magnitude of the largest potentially induced seismic event. *J Seismol* 18:421–431
- Healy JH, Rubey WW, Griggs DT, Raleigh CB (1968) The Denver earthquakes. *Science* 161:3848
- Hennings PH, Nicot JP, Gao RS, DeShon HR, Lund Snee JE, Morris AP, Brudzinski MR, Horne EA, Breton C (2021) Pore pressure threshold and fault slip potential for induced earthquakes in the Dallas-Fort Worth area of north central Texas. *Geophys Res Lett* 48:e2021GL093564
- Horton S (2012) Injection into subsurface aquifers triggers earthquake swarm in central Arkansas with potential for damaging earthquake. *Seismol Res Lett* 83:250–260

- Horner RB, Barclay JE, MacRae JM (1994) Earthquakes and hydrocarbon production in the Fort St. John area of northeastern British Columbia. *Can J Explor Geophys* 30:39–50
- Hosseini BK, Eaton DW (2018) Fluid flow and thermal modeling for tracking induced seismicity near the Graham disposal well, British Columbia (Canada). SEG 88th annual conference, Anaheim CA, expanded abstracts 4987–4991
- Improta L, Valoroso L, Piccinini D, Chiarabba C (2015) A detailed analysis of wastewater-induced seismicity in the Val d'Agri oil field (Italy). *Geophys Res Lett* 42:2682–2690
- Kao H, Hyndman R, Jiang Y, Visser R, Smith B, Mahani AB, Leonard L, Ghofrani H, He J (2018) Induced seismicity in western Canada linked to tectonic strain rate: implications for regional seismic hazard. *Geophys Res Lett* 45:11104–11115
- Kendall J-MA, Butcher AL, Stork JP, Verdon R, Luckett BJB (2019) How big is a small earthquake? Challenges in determining microseismic magnitudes. *First Break* 37:51–56
- Keranen KM, Savage HM, Abers GA, Cochran ES (2013) Potentially induced earthquakes in Oklahoma: USA: links between wastewater injection and the 2011  $M_w$  5.7 earthquake sequence. *Geology* 41:699–702
- Keranen KM, Weingarten M, Abers GA, Bekins BA, Ge S (2014) Sharp increase in central Oklahoma seismicity since 2008 induced by massive wastewater injection. *Science* 345:448–451
- Kettlety T, Verdon JP, Werner MJ, Kendall J-M, Budge J (2019) Investigating the role of elastostatic stress transfer during hydraulic fracturing-induced fault activation. *Geophys J Int* 217:1200–1216
- Kettlety T, Verdon JP, Butcher A, Hampson M, Craddock L (2021) High-resolution imaging of the  $M_L$  2.9 August 2019 earthquake in Lancashire, United Kingdom, induced by hydraulic fracturing during Preston New Road PNR-2 operations. *Seismol Res Lett* 92:151–169
- Kim W-Y (2013) Induced seismicity associated with fluid injection into a deep well in Youngstown, Ohio. *J Geophys Res* 118:3506–3518
- Kroll KA, Cochran ES (2021) Stress controls rupture extent and maximum magnitude of induced earthquakes. *Geophys Res Lett* 48:e2020GL092148
- Kwiatak G, Saamo T, Ader T, Bluemle F, Bohnhoff M, Chendorain M, Dresen G, Heikkinen P, Kukkonen I, Leary P, Leonhardt M, Malin P, Martinez-Garzon P, Passmore K, Passmore P, Valenzuela S, Wollin C (2019) Controlling fluid-induced seismicity during a 6.1-km-deep geothermal stimulation in Finland. *Sci Adv* 5:eaav7224
- Langenbruch C, Ellsworth WL, Woo J-U, Wald DJ (2020) Value at induced risk: injection-induced seismic risk from low-probability, high-impact events. *Geophys Res Lett* 47:e2019GL085878
- Lei X, Ma S, Chen W, Pang C, Zeng J, Jiang B (2013) A detailed view of the injection-induced seismicity in a natural gas reservoir in Zigong, southwestern Sichuan Basin, China. *J Geophys Res* 118:4296–4311
- Lei X, Wang Z, Su J (2019) The December 2018  $M_L$  5.7 and January 2019  $M_L$  5.3 earthquakes in South Sichuan Basin induced by shale gas hydraulic fracturing. *Seismol Res Lett* 90:1099–1110
- Lei X, Su J, Wang Z (2020) Growing seismicity in the Sichuan Basin and its association with industrial activities. *Science China* 63:1633–1660
- Li T, Gu YJ, Wang J, Wang R, Yusifbayov J, Reyes Canales M, Shipman T (2022) Earthquakes induced by wastewater disposal near Musreau Lake, Alberta, 2018–2020. *Seismol Res Lett* 93:727–738
- Mancini S, Werner MJ, Segou M, Baptie B (2021) Probabilistic forecasting of hydraulic fracturing-induced seismicity using an injection-rate driven ETAS model. *Seismol Res Lett* 92:3471–3481
- McGarr A, Barbour AJ (2017) Wastewater disposal and the earthquake sequences during 2016 near Fairview, Pawnee, and Cushing, Oklahoma. *Geophys Res Lett* 44:9330–9336
- McNamara DE, Hayes GP, Benz HM, Williams RA, McMahon ND, Aster RC, Holland A, Sickbert T, Herrmann R, Briggs R, Smoczyk G, Bergman E, Earle P (2015) Reactivated faulting near Cushing, Oklahoma: increased potential for a triggered earthquake in an area of United States strategic infrastructure. *Geophys Res Lett* 42:8328–8332
- Mendecki AJ (2016) Mine seismology reference book: seismic hazard. Institute of Mine Seismology, Tasmania, Australia
- Meremonte ME, Lahr JC, Frankel AD, Dewey JW, Crone AJ, Overturf DE, Carver DL, Rice WT (2002) Investigation of an earthquake swarm near Trinidad, Colorado, August–October 2001. US Geological Survey open-file report 02–0073
- Molina I, Velásquez JS, Rubenstein JL, Garcia-Aristizabal A, Dionicio V (2020) Seismicity induced by massive wastewater injection near Puerto Gaitán, Colombia. *Geophys J Int* 223:777–781
- Nakai JS, Weingarten M, Sheehan AF, Bilek SL, Ge S (2017) A possible causative mechanism of Raton Basin, New Mexico and Colorado earthquakes using recent seismicity patterns and pore pressure modelling. *J Geophys Res* 122:8051–8065
- Nicholson C, Roeloffs E, Wesson RL (1988) The Northeastern Ohio earthquake of 31 January 1986: was it induced? *Bull Seismol Soc Am* 78:188–217
- Roberts NS, Bell AF, Main IG (2015) A volcanic seismic b-values high, and if so when? *J Volcanol Geoth Res* 308:127–141
- Rodriguez-Pradilla G, Eaton DW, Verdon JP (2022) Basin-scale multi-decadal analysis of hydraulic fracturing and seismicity in western Canada shows non-recurrence of induced runaway fault rupture. *Scientific Reports*, accepted
- Rubenstein JL, Mahani AB (2015) Myths and facts on wastewater injection, hydraulic fracturing, enhanced oil recovery, and induced seismicity. *Seismol Res Lett* 86:1060–1067
- Savvaadis A, Young B, Huang GD, Lomax A (2019) TexNet: a statewide seismological network in Texas. *Seismol Res Lett* 90:1702–1715
- Schoenball M, Ellsworth WL (2017) Waveform-relocated earthquake catalog for Oklahoma and southern Kansas illuminates the regional fault network. *Seismol Res Lett* 88:1252–1258
- Schoenball M, Walsh FR, Weingarten M, Ellsworth WL (2018) How faults wake up: the Guthrie-Langston, Oklahoma earthquakes. *Lead Edge* 37:100–106
- Schultz R, Stern V, Gu YJ (2014) An investigation of seismicity clustered near the Cordel Field, west central Alberta,

- and its relation to a nearby disposal well. *J Geophys Res* 119:3410–3423
- Schultz R, Beroza G, Ellsworth W, Baker J (2020) Risk-informed recommendations for managing hydraulic fracturing-induced seismicity via traffic light protocols. *Bull Seismol Soc Am* 110:2411–2422
- Schultz R, Beroza GC, Ellsworth WL (2021) A risk-based approach for managing hydraulic fracturing-induced seismicity. *Science* 372:504–507
- Schultz R, Ellsworth WL, Beroza GC (2022) Statistical bounds on how induced seismicity stops. *Sci Rep* 12:1–11
- Seeber L, Armbruster JG, Kim W-Y (2004) A fluid-injection-triggered earthquake sequence in Ashtabula, Ohio: implications for seismogenesis in stable continental regions. *Bull Seismol Soc Am* 94:76–87
- Skoumal RJ, Brudzinski MR, Currie BS, Levy J (2014) Optimizing multi-station earthquake template matching through re-examination of the Youngstown, Ohio, sequence. *Earth Planet Sci Lett* 405:274–280
- Skoumal RJ, Ries R, Brudzinski MR, Barbour AJ, Currie BS (2018) Earthquakes induced by hydraulic fracturing are pervasive in Oklahoma. *J Geophys Res* 123:10918–10935
- Skoumal RJ, Barbour AJ, Brudzinski MR, Langenkamp T, Kaven JO (2020a) Induced seismicity in the Delaware Basin, Texas. *J Geophys Res* 125:e2019JB018558
- Skoumal RJ, Kaven JO, Barbour AJ, Wicks C, Brudzinski MR, Cochran ES, Rubinstein JL (2020b) The induced Mw 5.0 March 2020 West Texas seismic sequence. *J Geophys Res* 126:e2020JB020693
- Tang L, Lu Z, Zhang M, Sun L, Wen L (2018) Seismicity induced by simultaneous abrupt changes of injection rate and well pressure in Hutubi Gas Field. *J Geophys Res* 123:5929–5944
- Tata MN (1969) On outstanding values in a sequence of random variables. *Probab Theory Relat Fields* 12:9–20
- van der Elst NJ (2021) *B-positive*: a robust estimator of after-shock magnitude distribution in transiently incomplete catalogs. *Journal of Geophysical Research* 126:e2020JB021027
- van der Elst NJ, Page MT, Weiser DA, Goebel THW, Hosseini SM (2016) Induced earthquake magnitudes are as large as (statistically) expected. *J Geophys Res Solid Earth* 121:4575–4590
- Verdon JP (2013) Fractal dimension of microseismic events via the two-point correlation dimension, and its correlation with b values. *Proceedings of the 4<sup>th</sup> EAGE passive seismic workshop*, Amsterdam, CP-337–00022
- Verdon JP (2014) Significance for secure CO<sub>2</sub> storage of earthquakes induced by fluid injection. *Environ Res Lett* 9:064022
- Verdon JP, Bommer JJ (2021a) Green, yellow, red, or out of the blue? An assessment of traffic light schemes to mitigate the impact of hydraulic fracturing-induced seismicity. *J Seismol* 25:301–326
- Verdon JP, Bommer JJ (2021b) Comment on “Activation rate of seismicity for hydraulic fracture wells in the Western Canadian Sedimentary Basin” by Ghofrani and Atkinson (2020). *Bull Seismol Soc Am* 111:3459–3474
- Verdon JP, Baptie BJ, Bommer JJ (2019) An improved framework for discriminating seismicity induced by industrial activities from natural earthquakes. *Seismol Res Lett* 90:1592–1611
- Verdecchia A, Cochran ES, Harrington RM (2021) Fluid-earthquake and earthquake-earthquake interactions in Southern Kansas, USA. *J Geophys Res* 126:e2020JB020384
- Walsh FR, Zoback MD (2015) Oklahoma’s recent earthquakes and saltwater disposal. *Sci Adv* 1:1500195
- Walter JL, Chang JC, Dotray PJ (2017) Foreshock seismicity suggests gradual differential stress increase in the months prior to the 3 September 2016 M<sub>w</sub> 5.8 Pawnee earthquake. *Seismol Res Lett* 88:1032–1039
- Walter JL, Ogwari P, Thiel A, Ferrer F, Woelfel I, Chang JC, Darold AP, Holland AA (2020) The Oklahoma Geological Survey statewide seismic network. *Seismol Res Lett* 91:611–621
- Wang Z, Lei X, Ma S, Wang X, Wan Y (2020) Induced earthquakes before and after cessation of long-term injections in Rongchang gas field. *Geophys Res Lett* 47:e2020GL089569
- Weingarten M, Ge S, Godt JW, Bekins BA, Rubinstein JL (2015) High-rate injection is associated with the increase in U.S. mid-continent seismicity. *Science* 348:1336–1340
- Wyss M, Shimazaki K, Wiemer S (1997) Mapping active magma chambers by b values beneath the off-Ito volcano, Japan. *J Geophys Res* 102:20413–20422
- Yeck WL, Sheehan AF, Benz HM, Weingarten M, Nakai J (2016) Rapid response, monitoring and mitigation of induced seismicity near Greeley, Colorado. *Seismol Res Lett* 87:837–847
- Yoon CE, Huang Y, Ellsworth WL, Beroza GC (2017) Seismicity during the initial stages of the Guy-Greenbrier, Arkansas, earthquake sequence. *J Geophys Res* 122:9253–9274

**Publisher’s note** Springer Nature remains neutral with regard to jurisdictional claims in published maps and institutional affiliations.